J Solid State Electrochem (2011) 15:399–404
DOI 10.1007/s10008-010-1101-1

ORIGINAL PAPER

Synthesis and electrochemical properties of layered $LiNi_{0.5-x}Mn_{0.5-x}Co_{2x}O_2$ for lithium-ion battery from nickel manganese cobalt oxide precursor

Shumei Dou · Wenlou Wang

Received: 25 February 2010 / Revised: 24 April 2010 / Accepted: 10 May 2010 / Published online: 23 May 2010

Abstract A series of $LiNi_{0.5-x}Mn_{0.5-x}Co_{2x}O_2$ ($0 < 2x \leq 0.33$) compounds were prepared by solid-state reaction from nickel manganese cobalt oxides, and their characteristics were investigated by X-ray diffraction, X-ray photoelectron spectroscopy, and charge–discharge test. $LiNi_{0.5-x}Mn_{0.5-x}Co_{2x}O_2$ samples have single phase of layered structure with a space group of $R\bar{3}m$ for $2x$=0.02, 0.05, 0.10, 0.20, and 0.33. Both the lattice constants of *a*- and *c*-axis and Li/Ni mixing degree decreased with the increase in Co contents in samples. The valence states of Ni, Mn, and Co in the samples are predominantly +2, +4, and 3, respectively, with a small amount of Ni^{3+}, Mn^{3+}, and Co^{2+}. $LiNi_{0.475}Mn_{0.475}Co_{0.05}O_2$ gives excellent cycling performance in the voltage range of 2.5–4.4 V at the current rate of 20 and 100 mA g^{-1} over 50 cycles. High-rate capacity test of $LiNi_{0.34}Mn_{0.33}Co_{0.33}O_2$ shows that even at a current rate of 1,000 mA g^{-1}, stable capacity about 63 mAh g^{-1} is retained.

Keywords Lithium ion battery · Cathode material · Ni–Mn–Co oxide precursor · Solid-state reaction · Electrochemical performance

Introduction

The $Li_xC_6/Li_{1-x}CoO_2$ rechargeable batteries have been used as cathode materials because they meet most of the requirements such as high energy and high power density. However, $Li_{1-x}CoO_2$ has some disadvantages, such as the cost, toxicity, and safety. So much effort needs to be made to develop alternative lithium-insertion electrodes [1–4]. Partial substitution such as $LiNi_{0.5-x}Mn_{0.5-x}Co_{2x}O_2$ has been proven an effective method in modifying the crystal structure and improving the electrochemical performance [5–14]. These compounds have the layered α-$NaFeO_2$ structure and the oxidation state of Ni, Mn, and Co ions are +2, +4, and +3, respectively, from the first principle calculations and X-ray absorption measurements [15]. Thus, Ni^{2+} is the electrochemically active ion, while the Mn^{4+} ion with octahedral coordination helps to ensure the stability of the structure, and Co^{3+} suppresses the cation mixing between 3a and 3b sites. However, the increase in Co content results in the decrease in the capacity of the materials, while the high content of Ni leads to the cation mixing. Therefore, the contents of Ni, Co, and Mn need to be optimized for the best performance of the materials.

The synthesis methods widely used include solid-state reaction [16, 17], coprecipitation method [7, 8, 12, 14], sol-gel method [10], ultrasonic spray thermal decomposition [18], spray-dry method [9], and so on. However, the particle size and morphology cannot be controlled by traditional solid-state reaction method, and the degree of Li/Ni cation mixing cannot be minimized in nature. Although the coprecipitation method can reduce the degree of Li/Ni cation mixing, it should be very careful to control the synthesis conditions with coprecipitation method in order to avoid the oxidation of Mn^{2+}. In addition, although other emerging method such as ultrasonic spray thermal decomposition and spray-dry method can lead to either improve capacity retention characteristic or high achievable specific capacity, it is a multistep synthesis process that the methods cannot be used in the

S. Dou · W. Wang (✉)
Department of Chemical Physics,
The University of Science and Technology of China,
Hefei, Anhui 230026, People's Republic of China
e-mail: wlwang@ustc.edu.cn

commercial production. This stimulates us to explore a new simple method to prepare the solid solution in order to obtain high battery–active cathode material.

In the present study, a series of $LiNi_{0.5-x}Mn_{0.5-x}Co_{2x}O_2$ $(0 < 2x \leq 0.33)$ compounds were prepared with nickel manganese cobalt oxide precursors by a solid-state reaction. The structure and electrochemical properties were also investigated.

Experimental

$LiNi_{0.5-x}Mn_{0.5-x}Co_{2x}O_2$ was prepared by a Ni–Mn–Co oxide precursor route. The detailed processes were similar to the method in our previous paper [19]. A certain amount of $Ni(CH_3COO)_2{\bullet}4H_2O$, $Co(CH_3COO)_2{\bullet}2H_2O$ and $Mn(CH_3COO)_2{\bullet}4H_2O$ in various molar ratio were initially dissolved in deionized water to form homogeneous solution; then, water was removed by means of a rotary evaporator at 75 °C, and salt precipitate was made. The salt precipitate was ground and calcined at 800 °C for 12 h in air. The as-prepared precursor was mixed with $LiOH{\cdot}H_2O$ (AR, 95%) in stoichiometric proportions and pressed into pellet. The pellets were heated at 500 °C for 3 h in air, followed by annealing at 900 °C for 12 h to obtain $LiNi_{0.5-x}Mn_{0.5-x}Co_{2x}O_2$ powders.

Characterization XRD patterns were obtained using a Philips X'Pert PW 3373 diffractometer (monochromatized Cu K_α radiation). The contents of cations in precursors were measured by inductively coupled plasma atomic analysis (ICP, Atom scan Advantage). X-ray photoelectron spectroscopy (XPS) was performed on ESCALAB MK II with monochromatic Al K_α X-ray radiation at 1486.6 eV with C1s (284.6 eV) as the reference line.

Electrochemical test Charge and discharge profiles were collected by galvanostatically cycling between 2.5 and 4.4 V (Shenzhen Neware, BTS, China). For the preparation of cathode sheets, slurry was formed by mixing the active material, acetylene black, and binder (polyvinylideneuoride, dissolved in *N*-methyl-2-pyrrolidone) in a weight ratio of 75:20:5. The slurry was spread uniformly on aluminium foil. The electrodes were dried under vacuum at 120 °C for 10 h and then pressed under 60 MPa and weighted. 1 M $LiPF_6$ in a 1:1 ethylene carbonate/diethyl carbonate was used as electrolyte, and lithium foil was used as anode. A thin sheet of microporous polypropylene insulated the positive electrode from negative electrodes. Battery assembly was carried out in an argon-filled glove box.

Table 1 Chemical composition (wt.%) of the prepared precursor and product determined by ICP

2*x*	Ni	Co	Mn	Ni/Co/Mn
0.33	25.91	25.89	22.77	0.34:0.34:0.32
0.20	31.10	15.54	26.64	0.41:0.21:0.38
0.10	35.02	7.90	30.15	0.47:0.10:0.43
0.05	36.27	3.90	31.02	0.495:0.053:0.452
0.02	35.92	1.57	31.75	0.50:0.02:0.48

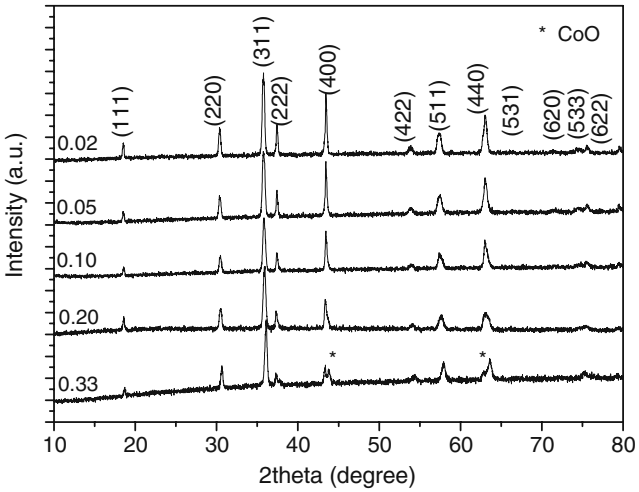

Fig. 1 XRD patterns of the Ni–Mn–Co oxide powders with different 2*x*

Results and discussions

The chemical compositions of the prepared precursors were determined by ICP, and the results are summarized in

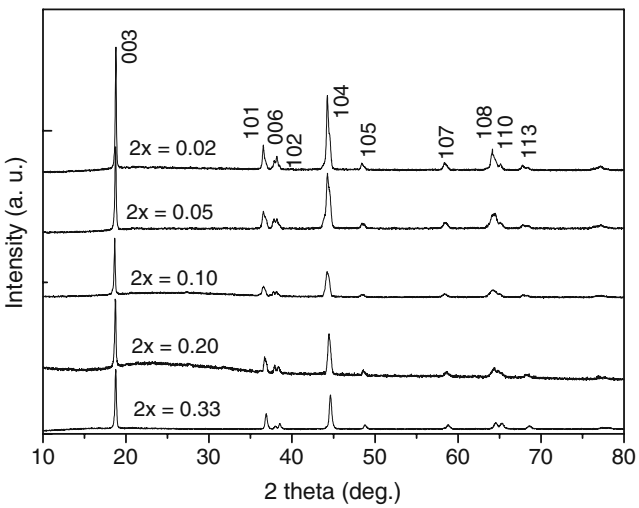

Fig. 2 XRD patterns of the $LiNi_{0.5-x}Mn_{0.5-x}Co_{2x}$ powders of different 2i

Table 2 Lattice constants, intensity ratios from Reitveld refinement for $LiNi_{0.5-x}Mn_{0.5-x}Co_{2x}O_2$

2x	*a* (Å)	*c* (Å)	*c*/*a*	Volume (Å^3)	$I_{(003)}/I_{(104)}$	R_p (%)	Li/Ni site exchange (%)
0.02	2.907	14.385	4.948	105.276	1.50	8.32	6.9
0.05	2.902	14.381	4.955	104.870	1.53	7.12	5.3
0.10	2.897	14.376	4.962	104.488	1.61	8.03	4.4
0.20	2.884	14.338	4.971	103.338	1.68	7.90	3.2
0.33	2.862	14.241	4.976	101.243	1.74	8.24	2.5

Table 1. The measured cation ratios of Ni/Co/Mn are almost the same as the designed values. The X-ray diffraction patterns of the precursors are shown in Fig. 1. It can be observed that, in addition to the precursor of $2x=0.33$, the rest of the precursors are confirmed to have a spinel $NiMn_2O_4$ (JCPDS card number 84-0542) structure. That is, Ni–Mn–Co oxide precursors can be obtained successfully with this method, ensuring sufficient mixing of Ni–Mn–Co in the precursor at the atomic level. However, the precursor with $2x=0.33$ contains some faint diffraction peaks of CoO phase, which implies that the metal oxide are heterogeneously reacted, and this may produce an effect on the structure and property of the final product to a certain extent.

The crystal structures of the $LiNi_{0.5-x}Mn_{0.5-x}Co_{2x}O_2$ materials with different $2x$ were investigated by XRD, as shown in Fig. 2. Diffraction patterns of all samples can be identified as a layered α-$NaFeO_2$ structure with a space group of $R\bar{3}m$. Distinct splitting of the (108)/(110) and (006)/(102) peaks are observed in these patterns, indicating that the layered $LiNi_{0.5-x}Mn_{0.5-x}Co_{2x}O_2$ cathode materials have been successfully synthesized for all the x in this experiment [20, 21]. In addition, the value of $I_{(003)}/I_{(104)}$ is used as a standard to measure the degree of the cation mixing in the layered compounds. The smaller the $I_{(003)}/I_{(104)}$ value is, the higher the disordering. Generally, the undesirable cation mixing takes place when $I_{(003)}/I_{(104)}<1.2$ [22, 23]. The $I_{(003)}/I_{(104)}$ values of all the samples in this work are larger than 1.2, as shown in Table 2, meaning that no undesirable cation mixing took place. As shown in Table 2, the lattice parameter, both *a*, related to average metal–metal intraslab distance, and *c*, correlated to the average metal–metal interslab distance, decreased with the molar ratio of Co increasing from 0.02 to 0.33. The increase in the content of Co^{3+} ion in the Mn site correspondingly decreases the Ni^{2+} ion content, resulting in shrinkage in the lattice volume [24]. Furthermore, the trigonal distortion, *c*/*a*, increased, and the *c*/*a* ratio of all the materials was observed to be above 4.94 for all samples, suggesting improved layered characteristics [24, 25]. The results of Rietveld refinement using Materials Studio 4.0 program for $2x=0.33$ are shown in Fig. 3. In the crystal structure analysis, it was assumed that the transition metals, Ni, Co, and Mn, equally occupied the 3b sites, Li occupied 3a sites, and oxygen was in the 6c sites [26]. During the refinement process, the occupancy of the 3b sites by Co and Mn was maintained at one third for each ion, and the total amount of Li and Ni within the materials was fixed. However, the distribution of Li and Ni between the 3a sites and 3b sites were allowed to vary. In this work, the degrees of Li/Ni cation mixing decreased with the increasing content of Co as shown in Table 2, evidencing that Co may stabilize the layered structure [27].

In order to elucidate the valence state of the transition metal species in the synthesized $LiNi_{0.5-x}Mn_{0.5-x}Co_{2x}O_2$ samples, XPS spectra were carried out as shown in Fig. 3. In the Ni XPS spectra, as shown in Fig. 3a, the major peak of Ni $2p_{3/2}$ peak at 854.6 eV, is near the binding energy of Ni^{2+} in NiO (854.1 eV) and far away from the binding energy of Ni^{3+} in $LiNiO_2$ (855.4 eV) [28, 29]. In addition, a characteristic satellite peak around 861.0 eV is also observed. Such a satellite is explained as due to the multiple splitting in the energy level of the Ni-containing oxides [29, 30]. Consequently, the conclusion can be drawn that the predominant oxidation states of Ni in the compounds are +2 with small content of Ni^{3+}. The XPS spectrum of Mn $2p_{3/2}$ shows the characteristic peak at 642.0 eV in Fig. 3b, which is closer to the value measured for Mn^{4+} in λ-MnO_2 (642.4 eV) than the value measured

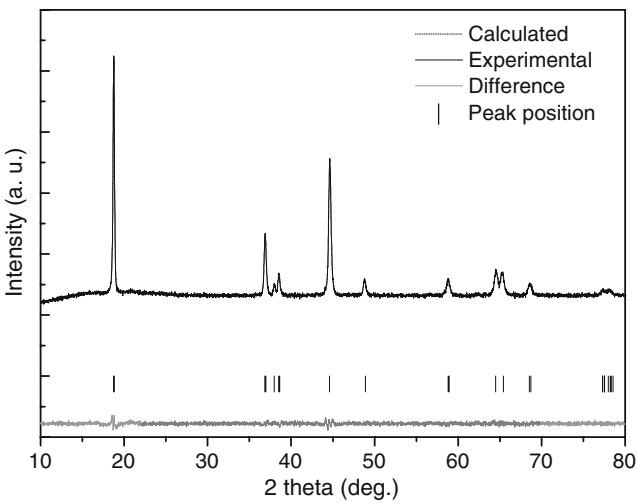

Fig. 3 XRD patterns of $LiNi_{0.34}Mn_{0.33}Co_{0.33}O_2$ phase by Reitveld refinement

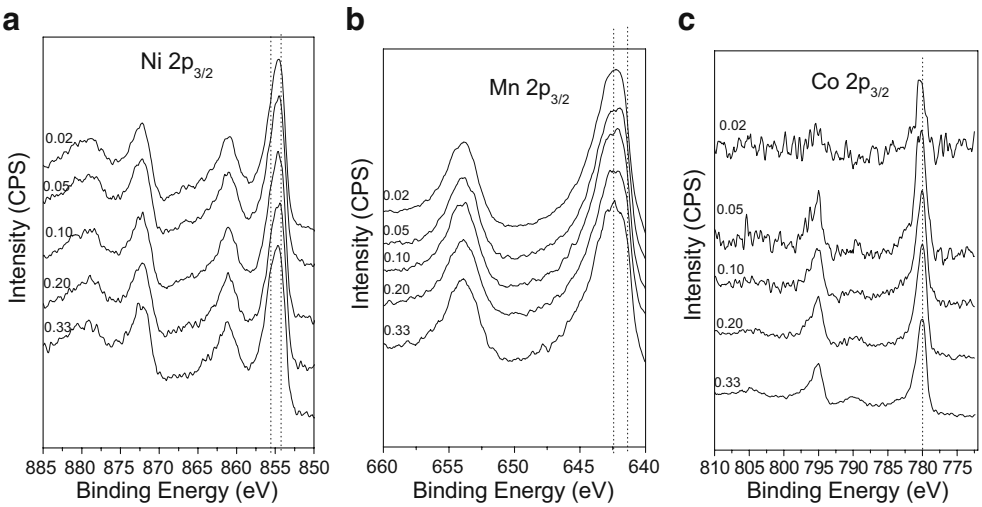

Fig. 4 XPS spectra of $LiNi_{0.5-x}Mn_{0.5-x}Co_{2x}O_2$: **a** Ni $2p_{3/2}$, **b** Mn $2p_{3/2}$ and **c** Co $2p_{3/2}$

for Mn^{3+} in $Li_2Mn_2O_4$ (641.4 eV) [31]. Therefore, the valences of the Mn in compounds were considered to be tetravalent and only trace of Mn^{3+}. The Co $2p_{3/2}$ spectra in Fig. 3c centered at 780.0 eV, which matches well with the value reported for Co^{3+} in $LiCoO_2$ [32, 33]. It is worth mentioning that the binding energy for lower cobalt content has a trend to shift to high energy, verifying that there is a minor contribution of Co^{2+}. A similar phenomena was observed in $LiNi_{1/3}Co_{1/3}Mn_{1/3}O_2$ [34]. Then, why can the behaviour of valency–degeneracy exist in compounds? Delmas et al. considered that it may be due to the electron transfer between M (Mn^{4+} or Co^{3+}) and Ni^{2+} or Ni^{4+} ions to Mn^{3+} or Co^{2+} and Ni^{3+} [35]. As Li_2MnO_3 does not appear in the XRD patterns, it is not the reason that Li substituted Ni^{2+} (3b) positions in the transition-metal layer compensate the charge balance [36] (Fig. 4).

The initial charge and discharge curves of $LiNi_{0.5-x}Mn_{0.5-x}Co_{2x}O_2$ cathodes with a constant current density of 20 mA g^{-1} between 2.5 and 4.4 V versus Li are shown in Fig. 5. All cells shows the same of the shape, smooth and monotonous charge/discharge curves, demonstrating that the manganese plays the role of an oxide network well performed for lithium intercalation [10]. The initial discharge capacities of the samples decreased with the content of cobalt increasing, which is not in agreement with the result of $Li(Ni_{0.5}Mn_{0.5})_{1-x}Co_xO_2$ $(0 \le x \le 0.33)$ reported by Sun et al. [18]. It is believed that the increase in cobalt content decreases the nickel content and thus reduces the discharge capacity.

Although the initial discharge capacity does not increase with the increase in the Co content, the cyclability of $LiNi_{0.5-x}Mn_{0.5-x}Co_{2x}O_2$ is ameliorated as shown in Fig. 6. When charged–discharged over 2.5–4.4 V for 50 cycles, the sample with $2x=0.02$ shows fast capacity fading, only 67.5% of its initial capacity remaining. While Co content $2x$ is increased to 0.05, the sample shows a capacity of 168 mAh g^{-1} and 86.1% of initial capacity retention after 50 cycles, exhibiting the best electrochemical performance among the samples. However, when the Co content $2x$ continues to increase to 0.33, the cyclability was not improved. The reason was probably due to the fact that the impurity phase of CoO in precursor resulted in the decrease of capacity retention because of the insufficiently mixing of Mn–Ni–Co in the precursor at the atomic level.

Figure 7 shows the discharge curves of the $LiNi_{0.5-x}Mn_{0.5-x}Co_{2x}$ electrodes with different $2x$ at a current rate of 100 mA g^{-1}. The reversible specific capacity increased with decreasing the content of cobalt. However, the electrodes with high content of cobalt have plateau area at a voltage range of 3.7–3.9 V, suggesting that they also showed stable constant power characteristic, even when they had low reversible specific capacity.

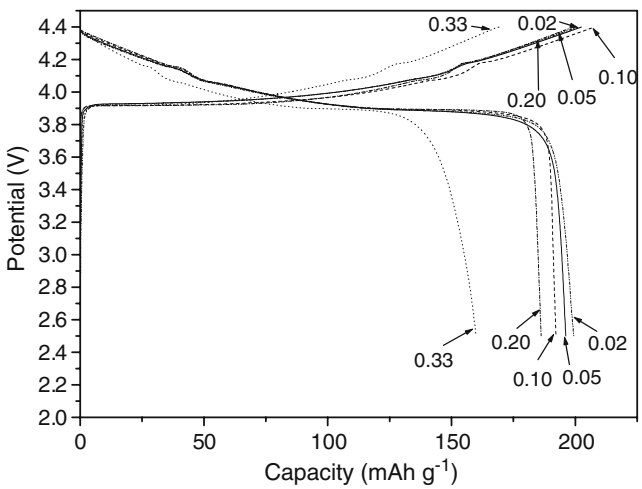

Fig. 5 Charge-discharge profiles of $LiNi_{0.5-x}Mn_{0.5-x}Co_{2x}O_2$ (voltage range, 2.5–4.4 V; current rate, 20 mA g^{-1})

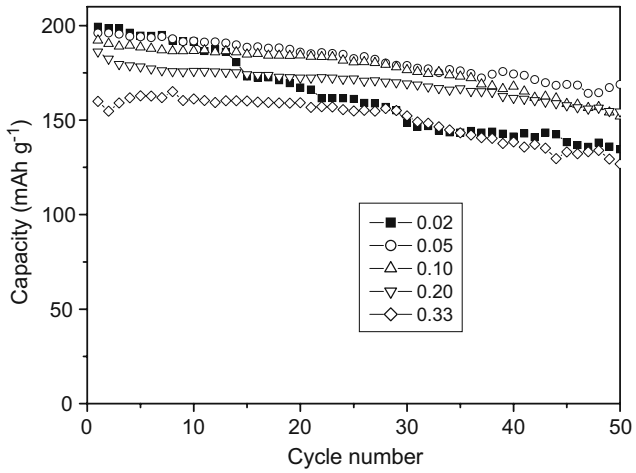

Fig. 6 Cycling performance of $LiNi_{0.5-x}Mn_{0.5-x}Co_{2x}O_2$ as a function of cycle number at a discharge rate of 20 mA g^{-1} between 2.5 and 4.4 V

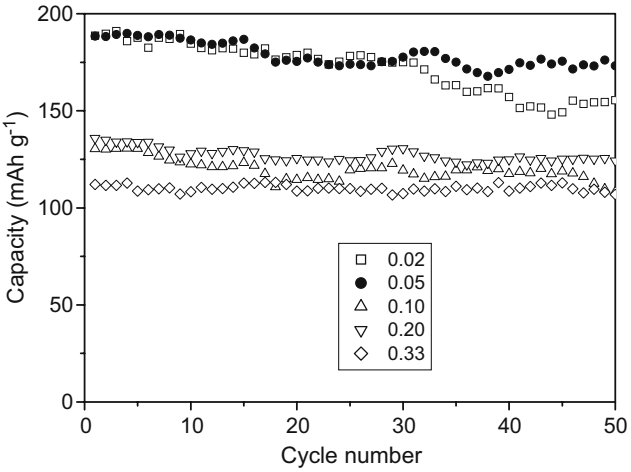

Fig. 8 Cycling performance of $LiNi_{0.5-x}Mn_{0.5-x}Co_{2x}O_2$ as a function of cycle number at a discharge rate of 100 mA g^{-1} between 2.5 and 4.4 V

Figure 8 shows the cycle performance of all samples at a constant current density of 100 mA g^{-1} at room temperature. In the voltage of 2.5–4.4 V, the sample with $2x=0.02$ delivered a capacity of 155 mAh g^{-1}, and the product with $2x=0.05$ delivered a comparing capacity of about 173 mAh g^{-1} after 50 cycles. This suggested that the partial substitution can improve the electrochemical performance remarkably, in the optimal amount range, which is mostly ascribed to the cation mixing as discussed above. Further increasing the content of cobalt resulted in a relatively lower capacity, which was due to the increase in cobalt content, decreases the nickel content. It is also found that the increase in cobalt content can enhance capacity retention. The capacity retention at the 50th cycles were 82.36%, 82.95%, and 95.39% for $2x=0.02$, 0.10, and 0.33, respectively. The improvement in cyclability by cobalt substituted was probably due to the ameliorated Li ion transportation associated with decreased degree of cation mixing [11].

Figure 9 shows the results of high-rate capacity tests accompanied with stability tests of $LiNi_{0.34}Mn_{0.33}Co_{0.33}$. The battery was charged at the same specific current of 20 mA g^{-1}. As shown in Fig. 9, for each 11 cycles at the same rate, the rate capacities scarcely changed. Even after 11 cycles at the rate of 1,000 mA g^{-1}, about 63 mAh g^{-1} remained. Compared with the literature [37], the capacity of $LiNi_{0.34}Mn_{0.33}Co_{0.33}O_2$ is too low, but it is reasonable because of the impurity in the precursor. When the discharge rate returns to 20 mA g^{m1}, the capacity is still about 157 mAh g^{-1}, which is almost its original value, after

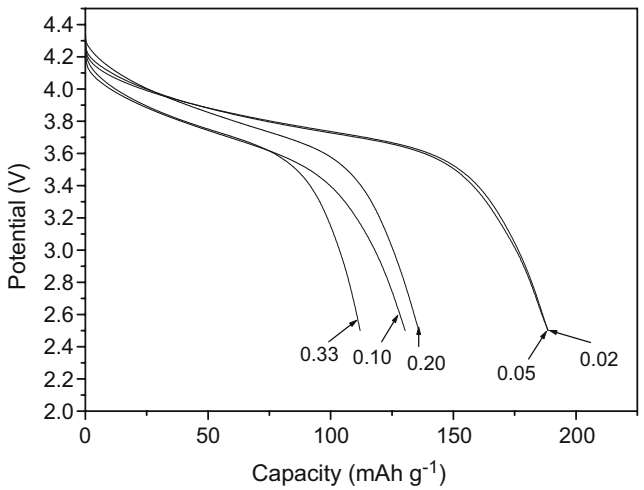

Fig. 7 Initial discharge curves of $LiNi_{0.5-x}Mn_{0.5-x}Co_{2x}O_2$ (voltage range, 2.5–4.4 V; current rate, 100 mA g^{-1})

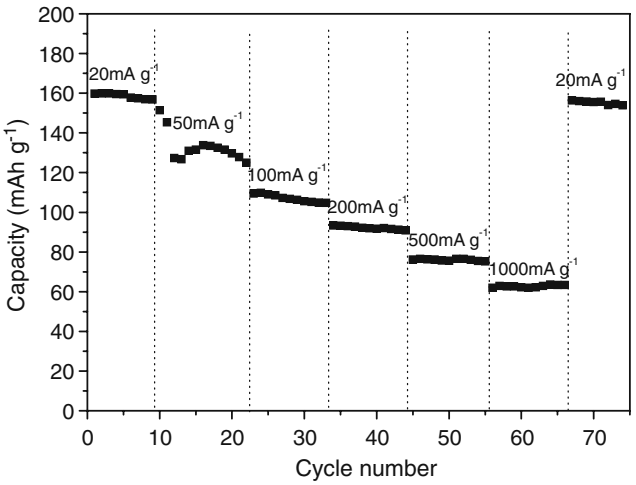

Fig. 9 Discharge capacity of $LiNi_{0.34}Mn_{0.33}Co_{0.33}O_2$ at different current with cycle number. The charge rate was fixed at 20 mA g^{-1}

completion of the high rates test, indicating that the as-prepared $LiNi_{0.34}Mn_{0.33}Co_{0.33}$ material has good electrochemical reversibility and structure stability. The high-rate discharge performance suggests that the synthesized $LiNi_{0.34}Mn_{0.33}Co_{0.33}$ composite would be well suitable for cathode materials of high power lithium batteries.

Conclusions

Layered $LiNi_{0.5-x}Mn_{0.5-x}Co_{2x}$ $(0 < 2x \leq 0.33)$ compounds have been prepared by solid-state reaction with Ni–Mn–Co oxide precursor. All samples are pure phase with layered structure of $R\bar{3}m$. The increase in cobalt content results in shrinkage in the lattice volume and slightly decreases the cation mixing. The partial substitution can improve the cycle performance. The $LiNi_{0.475}Mn_{0.475}Co_{0.05}O_2$ materials demonstrate excellent cycling performance in the voltage range of 2.5–4.4 V with good capacity retention at 20 and 100 mA g^{-1} over 50 cycles. High-rate capacity test of $LiNi_{0.34}Mn_{0.33}Co_{0.33}O_2$ shows that the as-prepared $LiNi_{0.34}Mn_{0.33}Co_{0.33}$ material has good electrochemical reversibility and structure stability.

Acknowledgement This work was supported by the foundation of the Department of Science and Technology, Anhui province.

References

1. Tarascon J-M, Armand M (2001) Nature 414:359–367
2. Xia Y, Takeshige H, Noguchi H, Yoshio M (1995) J Power Sources 56:61–67
3. Liu Z, Wan W-L, Liu X, Wu M, Li D, Zhen Z (2004) J Solid State Chem 177:1585–1591
4. Padhi AK, Nanjundaswamy KS, Goodenough JB (1997) J Electrochem Soc 144:1188–1194
5. Du F, Bie XF, Chen Y, Wei YJ, Liu LN, Wang CZ, Zou GT, Chen G (2009) J Appl Phys 106:053904
6. Lu CH, Lin YK (2009) J Power Sources 189:40–44
7. Shaju KM, Bruce PG (2006) Adv Mater 18:2330–2334
8. Choi J, Manthiram A (2006) J Power Sources 162:667–672
9. Li DC, Noguchi H, Yoshio M (2004) Electrochim Acta 50:427–430
10. Nithya C, Thirunakaran R, Sivashanmugam A, Kiruthika GVM, Gopukumar S (2009) J Phys Chem C 113:17936–17944
11. Ni JF, Zhou HH, Chen JT, Zhang XX (2008) Electrochim Acta 53:3075–3083
12. Chernova NA, Ma M, Xiao J, Whittingham MS, Breger J, Grey CP (2007) Chem Mater 19:4682–4693
13. Bentaleb Y, Saadoune I, Maher K, Saadi L, Fujimoto K, Ito S (2010) J Power Sources 195:1510–1515
14. Ma M, Chernova NA, Toby BH, Zavalij PY, Whittingham MS (2007) J Power Sources 165:517–534
15. Deb A, Bergman U, Cramer SP, Cairns EJ (2005) J Appl Phys 97:113523
16. Liao PY, Duh JG, Sheen SR (2005) J Power Sources 143:212–218
17. Gan CL, Hu XH, Zhan H (2005) Solid State Ion 176:687–692
18. Oh SW, Park SH, Park CW, Sun YK (2004) Solid State Ionics 171:167–172
19. Meng XL, Dou SM, Wang WL (2008) J Power Sources 184:489–493
20. Hwang BJ, Tsai YW, Carlier D, Ceder G (2003) Chem Mater 15:3676–3682
21. Chen CH, Wang CJ, Hwang BJ (2005) J Power Sources 146:626–629
22. Liu ZL, Yu AH, Lee JY (1999) J Power Sources 81–82:416–419
23. Ohzuku T, Ueda A, Nagayama M, Iwakoshi Y, Komori H (1993) Electrochim Acta 38:1159–1167
24. Hinuma Y, Meng YS, Kang K, Ceder G (2007) Chem Mater 19:1790–1800
25. Yoshio SM, Todorov Y, Yamato K, Noguchi H, Itoh J, Okada M, Mouri T (1998) J Power sources 74:46–53
26. Idemoto Y, Takanashi Y, Kitamura N (2009) J Power Sources 189:269–278
27. Wang L, Li JG, He XM, Pu WH, Wan CR, Jiang CY (2009) J Solid State Electrochem 13:1157–1164
28. Carley AF, Jackson SD, O'Shea JN, Roberts MW (1999) Surf Sci 440:L868–L874
29. Amine K, Tukamoto H, Yasuda H, Fujita Y (1996) J Electrochem Soc 143:1607–1613
30. Gopukumar S, Chung KY, Kim KB (2004) Electrochim Acta 49:803–810
31. Kang SH, Kim J, Stoll ME, Abraham D, Sun YK, Amine K (2002) J Power Sources 112:41–48
32. Madhavi S, Rao GVS, Chowdari BVR, Li SFY (2001) J Electrochem Soc 148:A1279–A1286
33. Galakhov VR, Kurmaev EZ, Uhlenbrock S, Neumann M, Kellerman DG, Gorshkov VS (1996) Solid State Commun 99:221–224
34. Shaju KM, Subba Rao GV, Chowdari BVR (2002) Electrochim Acta 48:145–151
35. Carlier D, Menetrier M, Delmas C (2001) J Mater Chem 11:594–603
36. Okamoto K, Shizuka K, Akai T, Tamaki Y, Okahara K, Nomura M (2006) J Electrochem Soc 153:A1120–A1127
37. Deng C, Zhang S, Wu B, Yang SY, Li HQ (2010) J Solid State Electrochem 14:871–875